Voltammetry and in situ scanning tunnelling spectroscopy of osmium, iron, and ruthenium complexes of 2,2 ':6 ',2 ''-terpyridine covalently linked to Au(111)-electrodes

ARTICLE *in* PHYSICAL CHEMISTRY CHEMICAL PHYSICS · JUNE 2011

Impact Factor: 4.49 · DOI: 10.1039/c1cp21197h · Source: PubMed

6 AUTHORS, INCLUDING:

Princia Salvatore
Leibniz-Institut für Analytische Wissenschaf…
8 PUBLICATIONS **41** CITATIONS
SEE PROFILE

Kasper Moth-Poulsen
Chalmers University of Technology
69 PUBLICATIONS **1,236** CITATIONS
SEE PROFILE

Richard Nichols
University of Liverpool
163 PUBLICATIONS **5,602** CITATIONS
SEE PROFILE

PCCP

Dynamic Article Links

Cite this: *Phys. Chem. Chem. Phys.*, 2011, **13**, 14394–14403

www.rsc.org/pccp

PAPER

Voltammetry and *in situ* scanning tunnelling spectroscopy of osmium, iron, and ruthenium complexes of 2,2′:6′,2′′-terpyridine covalently linked to Au(111)-electrodes†

Princia Salvatore,[a] Allan Glargaard Hansen,[a] Kasper Moth-Poulsen,[bc] Thomas Bjørnholm,[b] Richard John Nichols[d] and Jens Ulstrup*[a]

Received 15th April 2011, Accepted 31st May 2011
DOI: 10.1039/c1cp21197h

We have studied self-assembled molecular monolayers (SAMs) of complexes between Os(II)/(III), Fe(II)/(III), and Ru(II)/(III) and a 2,2′,6′,2′′-terpyridine (terpy) derivative linked to Au(111)-electrode surfaces *via* a 6-acetylthiohexyloxy substituent at the 4′-position of terpy. The complexes were prepared *in situ* by first linking the terpy ligand to the surface *via* the S-atom, followed by addition of suitable metal compounds. The metal-terpy SAMs were studied by cyclic voltammetry (CV), and *in situ* scanning tunnelling microscopy with full electrochemical potential control of substrate and tip (*in situ* STM). Sharp CV peaks were observed for the Os- and Fe complexes, with interfacial electrochemical electron transfer rate constants of 6–50 s^{-1}. Well-defined but significantly broader peaks (up to 300 mV) were observed for the Ru-complex. Addition of 2,2′-bipyridine (bipy) towards completion of the metal coordination spheres induced voltammetric sharpening. *In situ* STM images of single molecular scale strong structural features were observed for the osmium and iron complexes. As expected from the voltammetric patterns, the surface coverage was by far the highest for the Ru-complex which was therefore selected for scanning tunnelling spectroscopy. These correlations displayed a strong peak around the equilibrium potential with systematic shifts with increasing bias voltage, as expected for a sequential two-step *in situ* ET mechanism.

1. Introduction

Electrochemical single-molecule surface science of both non-redox and redox molecules including biological redox metalloproteins has evolved over the last few years.[1–18] In addition to high-resolution single-molecule imaging by electrochemical scanning tunnelling microscopy (*in situ* STM) in particular, redox molecules as "smarter" molecular units have offered other perspectives in tunnelling current/overpotential and tunnelling current/bias voltage spectroscopy (*in situ* scanning tunnelling spectroscopy, STS).[1–4,10–22] The most conspicuous feature in such correlations is a strong "spectroscopic" feature (maximum) close to the equilibrium redox potential, reflecting a two-step sequential interfacial electrochemical electron transfer (ET) mechanism. Perspectives and theoretical frames of these notions are now available[19–25] and have been reviewed recently.[19]

The duality of spectroscopic correlations, equivalent to single-molecule current/bias and current/gate voltage correlations in solid state transistor function, is unique to electrochemical *in situ* STM as opposed to *ex situ* STM in ultra-high vacuum or air environment. Transition metal complexes based on polypyridine ligands are here interesting molecular targets.[11–14] Merits of this class of potential single-molecule electronic components are, first that the complexes are robust to ligand substitution and stable in condensed matter environment in several electrochemically accessible oxidation states. Secondly, they offer a rich variety of options for electronic fine-tuning by using different central metal ions and combinations of pure and substituted polypyridine ligands. The resulting complexes can finally be immobilized on well-defined, atomically planar metal electrode surfaces and in well-defined structural configurations by use of suitable linker group substituents.[11–13,25]

Polypyridine transition metal complexes offer other new perspectives in single-molecule electrochemically based science. One perspective is that they have emerged as suitable molecular entities in the assembly of biological meso- and macromolecular units into metal-induced, "zipper-motifs" of chemically organized

[a] *Department of Chemistry, Technical University of Denmark, Building 207, DK-2800 Kongens Lyngby, Denmark. E-mail: ju@kemi.dtu.dk; Fax: 45 4588 3136; Tel: 45 4525 2359*
[b] *Nano-Science Center, Department of Chemistry, University of Copenhagen, DK-2100 Copenhagen, Denmark*
[c] *Chalmers University of Technology, Department of Chemical and Biological Engineering, SE-412 96 Gothenburg, Sweden*
[d] *Centre for Nanoscale Science, Chemistry Department, University of Liverpool, Liverpool L69 7ZD, United Kingdom*
† Electronic Supplementary Information (ESI) available. See DOI: 10.1039/c1cp21197h

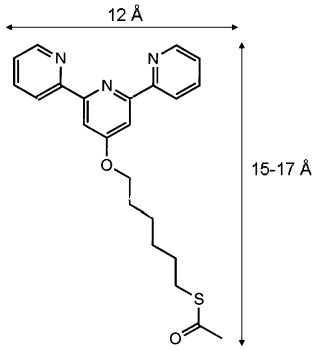

Fig. 1 Terpy with C6 linker group linker group, 4′-(6-acetylthiohexyloxy)-2,2′;6′2′′-terpy.

oligonucleotide duplex formation.[26] A second perspective is that polypyridine transition metal complexes can be brought to operate as *thermal* electrochemical ET markers at low energy,[27–29] as opposed to photo-induced long-range ET patterns of DNA-based molecules in particular.[28,30]

We report here a study of a class of transition metal complexes that offer both STS perspectives and a perspective as biomolecular markers as noted. 2,2′;6′,2′′-terpyridine (terpy) is the core ligand. This choice is prompted by the multichelate nature of the ligand that leaves at the same time ample choice for completion of the ligand sphere by other exogenous ligands. SAMs of the complexes are, secondly prepared *in situ* directly immobilized on single-crystal Au(111)-electrode surfaces. 4′-(6-acetylthiohexyloxy)-2,2′;6′2′′-terpyridine, terpy with C6 linker group (terpy-C6-SAc) (Fig. 1), was first synthesized and brought to SAM formation on the electrode surfaces. A suitable transition metal salt or metal complex (Os, Fe, Ru) was added next for coordination to the surface immobilized terpy moiety, followed by removal of excess metal compound. The three remaining vacant coordination sites (water, hydroxide, chloride, acetate) could be substituted by bipyridine or other exogenous ligands. This strategy has offered promising outcomes for *in situ* STM imaging and STS of the resulting surface confined transition metal based SAMs as well as for further use of this single-molecule strategy in redox marking of biological macromolecules.

2. Experimental

2.1 Target molecules and chemicals

Terpy with a 4′-(6-acetylthiohexyloxy) linker group (Fig. 1) was synthesised using a previously communicated method.[31] In brief, 2,6-bis-(pyrid-2-yl)-4-pyridone was reacted with 6-acetylthiol-1-bromohexane in DMF using potassium carbonate as a base.

Potassium hexachloro-osmate(IV) 99.99%, Fe(II)acetate 99.99% ($FeAc_2$) and Ruthenium(III) chloride hydrate 99.98% were all purchased from Aldrich. 2,2′-bipyridine 99.5% (bipy) was from Merck, 2,2′;6′,2′′-terpyridine 99% (terpy) from Sigma, and 6-Mercapto-1-hexanol 97% (MCH) from Aldrich.

The electrolyte solution (0.01 M, pH 7.0) was prepared from KH_2PO_4 (Sigma-Aldrich, 99.99%) and K_2HPO_4 (Fluka, 99.99%). KOH (99.99%) was used for reductive desorption and obtained from Sigma-Aldrich. Millipore water (conductivity of 18.2 kΩ cm) was used throughout. Absolute ethanol (EtOH) (extra pure, Sigma-Aldrich) was used as a solvent for the terpy compound, and the free ligands, bipy and terpy.

2.2 Electrochemistry

2.2.1 Electrodes. Single-crystal Au(111) bead electrodes (2–3 mm in diameter) were prepared as described[32,33] and used after electropolishing with H_2SO_4, removal of oxide with HCl, annealing in an oven at 860 °C for 8 h, followed by annealing in a H_2-flame and quenching in H_2-saturated water.

2.2.2 Sample preparation. About 1 mg of terpy-C6-SAc was dissolved in 1 ml EtOH leading to concentrations about 0.5 mM. Self-assembled full monolayers were prepared by immersing the annealed substrate electrodes in millimolar ethanolic solutions of terpy-C6-SAc for 1–20 h. After surface modification, the samples were removed from the terpy solution, rinsed with EtOH, and exposed to the metal compound (1–5 mM) in aqueous solution for 1–4 h. Excess metal compound was removed by rinsing with Millipore water.

The electrodes with metal-terpy monolayers were further soaked in millimolar ethanolic solution of bipy or terpy in order to replace remaining vacant (water or chloride) coordination sites of the metal.

Self-assembled mixed monolayers with the terpy-C6-SAc ligand embedded in a 6-mercaptohexanol (MCH) matrix were prepared in two ways. The gold electrodes were either exposed to MCH after immersion in terpy-C6-SAc solution (sequential adsorption), or directly immersed in a mixture of MCH and terpy-C6-SAc (simultaneous adsorption) for at least 1 h. Millimolar MCH solutions were used in both cases (1 mM MCH for sequential adsorption and 7.3 mM for coadsorption).

2.2.3 Cyclic voltammetry. Cyclic voltammograms were recorded using a 15 ml, three-compartment cell containing 0.01 M KH_2PO_4/K_2HPO_4 (pH 7.0) as electrolyte solution. A freshly prepared reversible hydrogen electrode (RHE) served as reference and a Pt wire as counter electrode. The electrolyte solution was degassed with pure Argon for 1 h prior to electrochemical experiments. All voltammetric measurements were carried out at room temperature, using an electrochemical Autolab PGSTAT12 system controlled by the GPES 4.9 software (Eco Chemie, Netherlands). The reference electrode was calibrated against a saturated calomel electrode (SCE) after each experiment. Electrochemical potentials are reported *versus* SCE.

2.3 Scanning tunnelling microscopy and scanning tunnelling spectroscopy

2.3.1 Instrumentation, sample preparation and *in situ* STM imaging. A PicoSPM *in situ* STM microscope was used. The same bead electrodes as for the electrochemical study was used as *in situ* STM substrates. Commercial disc Au(111) electrodes (SPL, The Netherlands & MaTeck, Germany) were employed in the STS measurements. A 3 ml Teflon house-built liquid cell was used. Platinum wires operated as reference and counter electrodes. The latter was calibrated against a saturated calomel electrode (SCE) after each experiment. Electrochemically etched

Pt/Ir tips (80/20, ∅ 0.25 mm) coated with Apiezon wax served as scanning probe.

STM Samples were prepared as above, only they were not quenched in H_2 saturated Millipore water, but held just above a Millipore water surface for approximately two minutes, before being transferred to the soaking solution. Low tunnelling currents (0.04–0.10 nA) and modest bias voltages (0.4 V) were generally used. Sample potentials were between −0.10 V and 0.20 V *vs.* SCE. I and P gains were in the range 2–5.

2.3.2 Scanning tunnelling spectroscopy. Before the recording of a scanning tunnelling spectrum the tip was positioned at a height above the sample surface decided by the set point tunnelling current (0.4 nA) and sample bias (−0.50 V). The feedback loop was then switched off and the working electrode potential scanned at a speed of 240–400 mV/s. The spectra shown are an average of at least fifty individual scans.

3. Results

We address first CV of the variably metal-coordinated terpy-C6-SAc mono- or sub-monolayers. This will be followed by *in situ* STM imaging of the sub-monolayers of the Os- and Fe-complexes and *in situ* STS of the Ru-based monolayers.

3.1 CV of full and MCH-mixed monolayers

We consider monolayers and sub-monolayers based on the three metals separately. As a reference, Fig. 2 shows a CV of immobilized free terpy-ligand on a Au(111)-electrode surface in 0.1 M KOH in the strongly negative potential region. The dominating feature is a strong peak at −1.02 V (*vs.* SCE) with a much smaller satellite peak at −1.06 V (*vs.* SCE). These potentials are in the Au-S reductive desorption region and suggest that terpy-C6-SAc is strongly bound either in the chemical state added or hydrolyzed and bound *via* a thiolate (thiyl) link. The coverage determined from the peak area is 6.4×10^{-10} mol/cm^2 corresponding to each terpy-C6-SAc molecule occupying an area of 26 Å^2. This is close to a full monolayer.

3.1.1 Os/terpy-C6-SAc monolayers. Fig. 3 shows CVs of pure terpy-C6-SAc (thiyl) monolayers, and terpy-C6-SAc monolayers exposed to $[OsCl_6]^{2-}$, or sequentially exposed to $[OsCl_6]^{2-}$

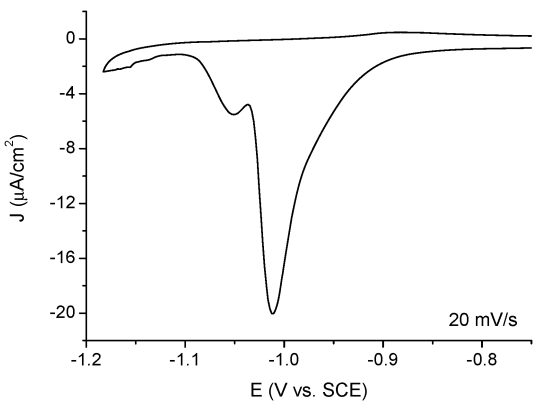

Fig. 2 Reductive desorption CV of terpy ligand from a Au(111)-electrode surface in 0.1 M KOH (pH 13.0). Scan rate 20 mV s^{-1}.

and exogenous ligands, terpy or bipy. No voltammetric peaks of the terpy-C6-SAc ligand itself were apparent in the potential range from −0.35 to +0.45 V. A pair of sharp voltammetric peaks at about +50 mV was observed after ligand monolayer exposure to $[OsCl_6]^{2-}$. The potential accords with expectations for Os(II)/(III) partially coordinated to polypyridine ligands. The sharp voltammetric peak appearance suggests a rather well-defined surface-confined coordination chemical complex. The anodic and cathodic peak areas are different but this is not uncommon even for robust complexes. This may reflect different surface orientations or ligand environments of the oxidized and reduced forms of the complexes and consequent difficulties in the precise subtraction of a capacitive background.

Addition of exogenous terpy showed no significant effects on the Os/terpy-C6-SAc voltammetric signals. The absence of any positive potential shift is indicative that the externally added terpy ligand is not coordinated under the conditions used which is in turn associated with the steric demands of this voluminous tridentate ligand. Addition of bipy with a view of formation of a surface-confined penta-coordinated Os/terpy-C6-SAc complex, however, induced a clear shoulder in the anodic part of the voltammogram. Two anodic peaks and the absence of a conspicuous cathodic counterpart reflect, on the other hand incomplete surface bipy-coordination and the presence of at least two species on the surface.

The voltammetric signals display the key features of monolayer voltammetry, linear peak height/scan rate dependence in particular. Coverage of metal-coordinated complexes is, however, in the range of only 10–30% in all cases. These relatively low values can be associated with the known substitution inert character of Os-complexes and perhaps with the complicated chemistry of the substitution process that also appears to involve redox chemistry in which added $[Os(IV)Cl_6]^{2-}$ complex is engaged. Peak separation at larger scan rates enabled undertaking kinetic analysis and obtaining the interfacial electrochemical ET rate constants. Results of this

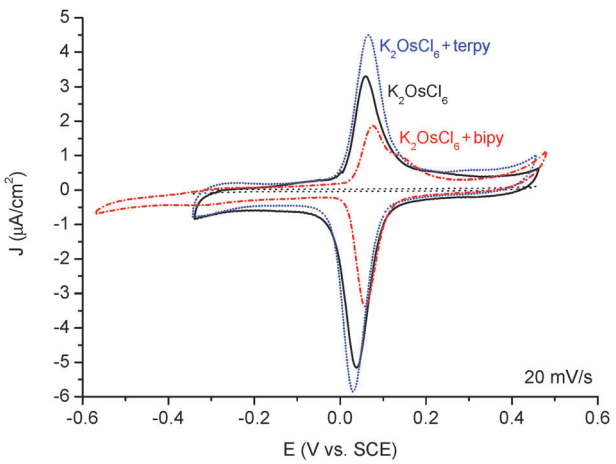

Fig. 3 CVs of terpy-C6-SAc (70 h) (**dotted line**), terpy-C6-SAc (24 h) + K_2OsCl_6 (22 h) (**solid**), terpy-C6-SAc (20 h) + K_2OsCl_6 (2.3 h) + terpy (2.4 h) (**short dot**), and terpy-C6-SAc (18 h) + K_2OsCl_6 (2.2 h) + bipy (2.3 h) (**short dash dot**) on a Au(111) electrode in 0.01 M KH_2PO_4/K_2HPO_4 (pH 7.0). Scan rate 20 mV s^{-1}.

Table 1 Kinetic and electrochemical data for the *in situ* assembled Os-complexes derived from statistics

	terpy-C6-SAc	Os-terpy-C6-SAc	terpy-Os-terpy-C6-SAc	bipy-Os-terpy-C6-SAc
$E^{0\prime}$/mV	0	60	34	67
ΔE_p/mV	0	30	25	16
Γ_a/μC cm^{-2}	0	10.5 (17%)	14.3 (23%)	9.2 (15%)
Γ_c/μC cm^{-2}	0	13.3 (21%)	16.8 (27%)	11.0 (18%)
k_{ET}/s^{-1}	0	6.0	6.0	7.9
$E_{p/2,\ a}$/mV (at 20 mV s^{-1})		65	70	73
$E_{p/2,\ c}$/mV (at 20 mV s^{-1})		60	62	53

analysis are given in Supporting Information. Redox potential ($E^{0\prime}$), peak separation (ΔE_p), surface coverage (Γ), ET rate constant (k_{ET}), and peak widths at half current height ($E_{p/2}$) are listed in Table 1. Subscripts a and c denote the anodic and cathodic peak, respectively.

The basic voltammetric features of saturated (10–30%) Os/terpy-C6-SAc sub-monolayers are paralleled by mixed Os/terpy-C6-SAc/MCH monolayers in the absence (Fig. 4) and presence (Fig. 5) of exogenous bipy ligand. Although slight, the differences between mixed monolayers prepared by sequential terpy-C6-SAc adsorption followed by MCH partial displacement and mixed monolayers prepared by co-adsorption, reflect the subtle control needed in the preparation of mixed adlayers with molecular function retained. The presence of a voltammetric "shoulder" again testify to the presence of two surface species after exposure to exogenous bipy ligand in the otherwise functional monolayers. The two species show quite similar interfacial electrochemical ET rate constants. Coverages are again notably smaller than for full monolayers, but electrochemical ET function is obviously retained. This is also reflected in the kinetic ET data for the mixed Os/terpy-C6-SAc/MCH electroactive monolayers summarized in Table 2 and 3.

3.1.2 Fe/terpy-C6-SAc monolayers. Fig. 6 shows voltammograms of surface-confined terpy-C6-SAc monolayers on Au(111)-electrode surfaces after exposure to 1 mM $FeAc_2$, and to sequential exposure to $FeAc_2$ and terpy or bipy. Clear and symmetric peaks are displayed, although broader than for the Os-complexes. The coverage is, however, even smaller than for the Os-complexes and in fact only a few percent. There is no immediate obvious reason why the Fe-terpy coverage should be so low. It could be suggested that Fe(II) added is oxidized to partially hydrolyzed substitution inert Fe(III)-species. The ligand substitution process might be optimized towards higher coverage for example by adjusting pH towards lower values. Peak separation is apparent at high scan rates (Supporting Information) and appropriate kinetic data are summarized in Table 4.

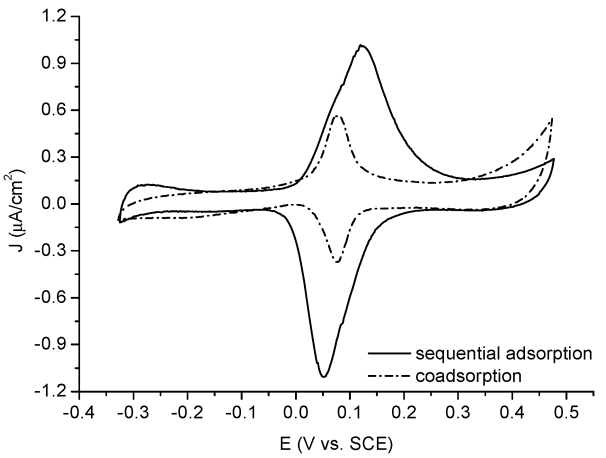

Fig. 4 CVs of (**solid curve**) sequentially adsorbed terpy-C6-SAc (20 h) + MCH (0.5 h) + K_2OsCl_6 (2.5 h) and (**dash dot**) of coadsorbed terpy-C6-SAc and MCH (0.5 h) + K_2OsCl_6 (1 h) on a Au(111) electrode in 0.01 M KH_2PO_4/K_2HPO_4 (pH 7.0). Scan rate 20 mV s^{-1}.

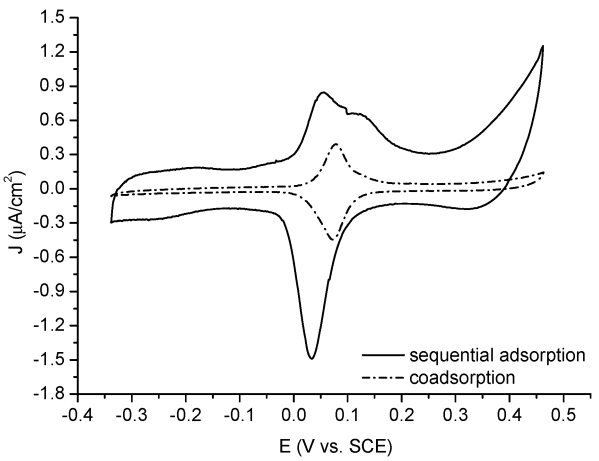

Fig. 5 CVs of (**solid curve**) sequentially adsorbed terpy-C6-SAc (20 h) + MCH (0.5 h) + K_2OsCl_6 (2.5 h) + bipy (2 h) and (**dash dot**) of coadsorbed terpy-C6-SAc and MCH (1.5 h) + K_2OsCl_6 (2.5 h) + bipy (0.8 h) on a Au(111) electrode in 0.01 M KH_2PO_4/K_2HPO_4 (pH 7.0). Scan rate 20 mV s^{-1}.

3.1.3 Ru/terpy-C6-SAc monolayers. Fig. 7 shows CVs of the terpy-C6-SAc monolayers, at a scan rate of 20 mV s^{-1} after exposure to 1 mM aqueous $RuCl_3$ solution, on a Au(111)-electrode, in 0.01 M KH_2PO_4/K_2HPO_4 (pH 7.0). Clear voltammetric signals are apparent, although significantly broader and with a character of multiple speciation compared with the Os- and Fe- complexes. This is also reflected in the much higher apparent coverage in excess of 100%. The effect of bipy addition is, however, both to induce a conspicuously sharper character on the voltammograms and to lower the coverage to values much closer to a single monolayer (Fig. 7). Both are indicative of the formation of a better defined surface-confined coordination chemical environment than without the exogenous bipy ligand added. The voltammetric and interfacial electrochemical ET data are summarized in Table 5. The values of the interfacial electrochemical ET rate constants of

Table 2 Kinetic and electrochemical data for the *in situ* assembled mixed Os-complex/MCH monolayers derived from statistics

Os-terpy-C6/MCH		
	Sequential adsorption	Simultaneous adsorption
$E^{0\prime}$/mV	85	77
ΔE_p/mV	70	2
Γ_a/μC cm^{-2}	5.63 (9.1%)	1.56 (2.5%)
Γ_c/μC cm^{-2}	4.82 (7.8%)	0.87 (1.4%)
k_{ET}/s^{-1}	14.1	26.2
$E_{p/2,\ a}$/mV (at 20 mV s^{-1})	117	51
$E_{p/2,\ c}$/mV (at 20 mV s^{-1})	84	44

Table 3 Kinetic and electrochemical data for the *in situ* assembled mixed Os-complex/MCH monolayers exposed to bipy derived from statistics

bipy-Os-terpy-C6/MCH		
	Sequential adsorption	Simultaneous adsorption
$E^{0\prime}$/mV	44	76
ΔE_p/mV	22	6
Γ_a/μC cm^{-2}	3.57 (5.8%)	1.12 (1.8%)
Γ_c/μC cm^{-2}	4.51 (7.3%)	1.27 (2.0%)
k_{ET}/s^{-1}	13.1	20.1
$E_{p/2,\ a}$/mV (at 20 mV s^{-1})	123	46
$E_{p/2,\ c}$/mV (at 20 mV s^{-1})	60	53

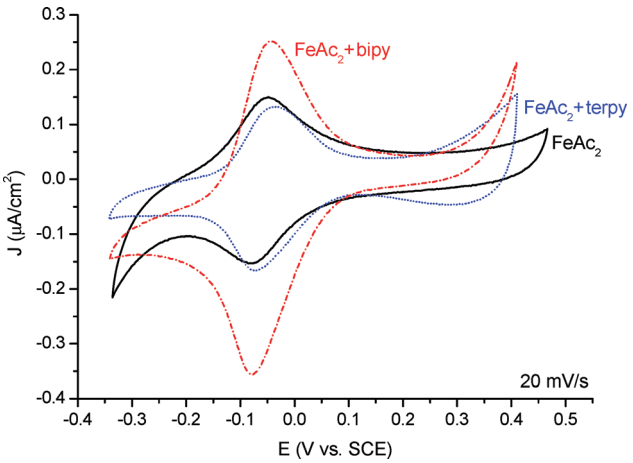

Fig. 6 CVs of terpy-C6-SAc (20 h) + $FeAc_2$ (3.2 h) (**solid line**), terpy-C6-SAc (19 h) + $FeAc_2$ (1.6 h) + terpy (3.0 h) (**short dot**), and terpy-C6-SAc (19 h) + $FeAc_2$ (1.6 h) + bipy (1.6 h) (**short dash dot**) on a Au(111)-electrode in 0.01 M KH_2PO_4/K_2HPO_4 (pH 7.0). Scan rate 20 mV s^{-1}.

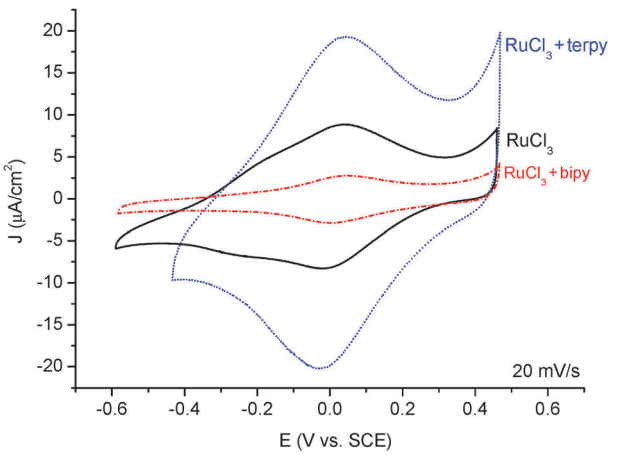

Fig. 7 CVs of terpy-C6-SAc (20 h) + $RuCl_3$ (4.5 h) (**solid line**), terpy-C6-SAc (19 h) + $RuCl_3$ (2.1 h) + terpy (5.3 h) (**short dot**), and terpy-C6-SAc (17.5 h) + $RuCl_3$ (2.2 h) + bipy (2.3 h) (**short dash dot**) on an Au(111) electrode in 0.01 M KH_2PO_4/K_2HPO_4 (pH 7.0). Scan rate 20 mV s^{-1}.

the three surface-confined metal-terpy complexes are rather similar and in the range 5–50 s^{-1}. We shall discuss this observation in Section 4. The data will be compared with *in situ* STM imaging and *in situ* STS in Section 3.2.

3.2 *In situ* STM imaging and *in situ* STS of surface-confined metal-coordinated terpy-C6-SAc SAMs

The voltammetric data strongly testify to the value of the *in situ* preparative approach to functional metal coordination

Table 4 Kinetic and electrochemical data for the *in situ* assembled Fe complexes derived from statistics

	Fe-terpy-C6-SAc	terpy-Fe-terpy-C6-SAc	bipy-Fe-terpy-C6-SAc
$E^{0\prime}$/mV	−65	−37	−68
ΔE_p/mV	21	35	25
Γ_a/μC cm^{-2}	0.84 (1.4%)	0.42 (0.7%)	2.64 (4.3%)
Γ_c/μC cm^{-2}	0.53 (0.9%)	0.38 (0.6%)	2.60 (4.3%)
k_{ET}/s^{-1}	50	22	19
$E_{p/2,\ a}$/mV (at 20 mV s^{-1})	126	116	124
$E_{p/2,\ c}$/mV (at 20 mV s^{-1})	109	116	118

Table 5 Kinetic and electrochemical data for *in situ* assembled Ru complexes derived from statistics

	Ru-terpy-C6-SAc	terpy-Ru-terpy-C6-SAc	bipy-Ru-terpy-C6-SAc
$E^{0\prime}$/mV	10	11	24
ΔE_p/mV	30	46	36
Γ_a/μC cm^{-2}	119 (241%)	140 (230%)	40 (65%)
Γ_c/μC cm^{-2}	112 (226%)	147 (241%)	40 (65%)
k_{ET}/s^{-1}	4.0	2.9	6.2
$E_{p/2,\ a}$/mV (at 20 mV s^{-1})	340	306	214
$E_{p/2,\ c}$/mV (at 20 mV s^{-1})	386	310	245

chemical compounds in confinements on well-defined, atomically planar Au(111)-electrode surfaces. In this section we address an equally powerful approach to the single-molecule characterization of the surface-confined metal complexes using *in situ* STM imaging and *in situ* STS.

3.2.1 *In situ* STM of pure and *in situ* Os- and Fe-coordinated terpy-C6-SAc SAMs. Fig. 8–11 show representative *in situ* STM images of the pure immobilized terpy-C6-SAc ligand (Fig. 8) and of the ligand monolayer after exposure to $[OsCl_6]^{2-}$ (Fig. 9 and 10) or $FeAc_2$ solution (Fig. 11). The image in Fig. 8 shows a dense adlayer, substantiating the high coverage disclosed by the reductive CV signal (Fig. 2). Molecular scale structures could not be observed under potential conditions where imaging was stable. Both molecular scale pits and larger domains of coalesced pits were, however, observed reflecting strong Au-S interaction as for electrochemical reductive desorption.

Fig. 9, upper shows an *in situ* STM image of the terpy-C6-SAc adlayer after exposure to 1 mM $[OsCl_6]^{2-}$. Strong, molecular scale contrasts are now scattered over the surface on an otherwise featureless but dense background. Fig. 9, lower shows a height profile of the molecular scale structures. The coverage and lateral size of the structures accord approximately with the coverage determined by the voltammetric data and with the expectable structural size of the surface-confined metal complexes, respectively. The apparent height difference between the bright spots and the metal-free terpy background is not widely different from the expected molecular structural difference. Identification of apparent height with real height, however, requires that the tunnelling mechanisms are the same for the Os-complex and the metal-free ligand. This assumption cannot be taken as valid due to the presence of a low-lying electronic redox level

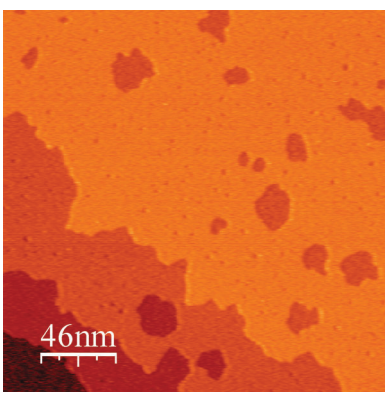

Fig. 8 *In situ* STM of terpy-C6-SAc (70 h) on a Au(111)-electrode surface in 0.01 M KH_2PO_4/K_2HPO_4 (pH 7.0). E_{work} = 0.04 V, E_{bias} = −0.42 V, I_{tunnel} = 0.040 nA.

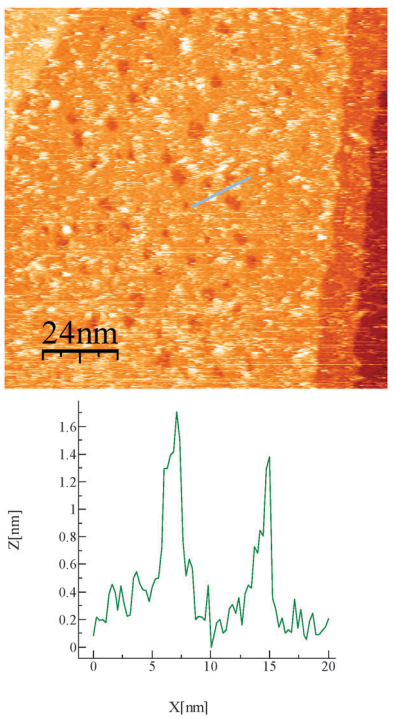

Fig. 9 *In situ* STM of terpy-C6-SAc (18 h) on a Au(111) electrode further functionalized with K_2OsCl_6 (2 h) in 0.01 M KH_2PO_4/K_2HPO_4 (pH 7.0). E_{work} = 0.13 V, E_{bias} = −0.35 V, I_{tunnel} = 0.100 nA (upper). Height profile along the light blue line in the image to the left (lower).

in the Os-complex but not in the metal-free ligand group. The Os-complex centre opens a two-step hopping mechanism in the potential range around the equilibrium potential. This is not feasible for the redox inactive metal-free ligand for which tunnelling or superexchange prevails. This point is supported by the strong STS spectrum of the Ru-complex with voltammetric peaks almost at the same potential as for the Os-complex, *cf.* Section 3.2.2.

The molecular scale structures can be recognized in the *ex situ* (ambient air environment) STM image (Fig. 10). The size and surface distribution follows the observations from the *in situ* STM image shown in Fig. 9, suggesting common features in the tunnelling mechanism in the two quite different environments.

The lateral size and the seven times apparent height rise (as in Fig. 9) that reflects a local tunnelling current rise strongly suggest that the sharp contrasts observed indeed arise from the Os-complexes in both the *ex situ* and *in situ* STM modes. The mechanism of electron tunnelling through a redox molecule is thus widely different and much more efficient compared with

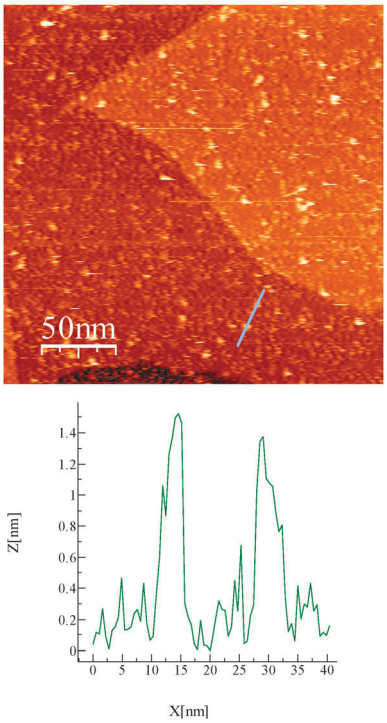

Fig. 10 *Ex situ* STM of a mixed monolayer of terpy-C6-SAc and MCH coadsorbed (0.5 h) on a Au(111)-electrode surface and further functionalized by 1 mM K_2OsCl_6 (1 h) in 0.01 M KH_2PO_4/K_2HPO_4 (pH 7.0). $E_{bias} = -0.42$ V, $I_{tunnel} = 0.040$ nA.

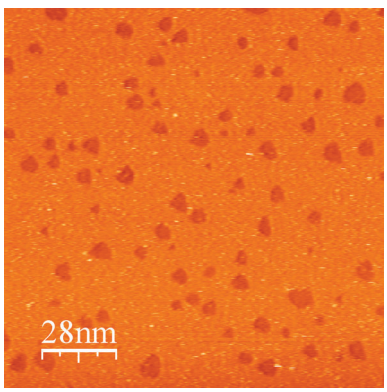

Fig. 11 *In situ* STM of terpy-C6-SAc (20 h) on a Au(111)-electrode surface further functionalized by $FeAc_2$ (2 h) in 0.01 M KH_2PO_4/K_2HPO_4 (pH 7.0). $E_{work} = 0.20$ V, $E_{bias} = -0.70$ V, $I_{tunnel} = 0.035$ nA.

tunnelling through non-redox molecular matter. These tunnelling mechanisms have been the subject of comprehensive studies.[1–4,11,12,19–25,33] We shall return briefly to this issue in the context of the present data in Sections 3.2.2 and 4. The *in situ* (and *ex situ*) STM data support the voltammetric data regarding the surface coverage of the Os-complexes. Other notable observations are that the terpy-C6-SAc monolayers, but not the Os-complexes, form dense monolayers but the Os-complexes appear to be broadly evenly distributed over the surface on a uniform background of uncoordinated ligand molecules. No tendency of formation of separate domains is thus apparent.

Fig. 11 shows a representative *in situ* STM image of terpy-C6-SAc (20 h) on a Au(111)-electrode surface after exposure to 1 mM $FeAc_2$. The image shows a dense adlayer with occasional sharper contrasts. These are, however, few in number and not conclusive as to their origin. The presence of conspicuous pits ranging in size from single-molecular size to coalesced larger sizes is, however, notable. The equilateral triangular shape of many of the pits is further notable.

The image accords in a sense with the voltammetric observations that disclosed clear voltammetric signals but very low Fe-coordinated complex surface concentrations. As noted, these shortcomings could be associated with incomplete surface preparation protocols for the Fe-complex. This could be worked on towards optimization of the iron complex as a target system in further single-molecule based efforts.

3.2.2 *In situ* STS of *in situ* prepared Ru/terpy-C6-SAc SAMs. The voltammetric data have shown that both osmium and iron can be brought to *in situ* coordination with surface-immobilized terpy-C6-SAc ligand molecules. With the preparation conditions used, the Os-complex can, however, be brought to coordinate in much higher surface coverage than the Fe-complex as shown by both voltammetry and *in situ* STM imaging. With a view on wider applications where the terpy ligand is combined with biological molecules, Os-terpy coordination chemistry rather than Fe-terpy therefore emerges as the more promising route on which to base such perspectives. This observation appears at first somewhat unexpected as Os-based coordination is renowned for robust chemical ligand substitution. Analogous ruthenium coordination chemistry is known to display faster ligand substitution and has been shown to be more suitable for biological redox marking of metalloproteins in particular.[34–36]

We therefore also addressed Ru-binding to Au(111)-surface immobilized terpy-SAc monolayers. As noted, exposure to aqueous (1 mM) $RuCl_3$ solution in fact gave strong but broad and not so immediately well-defined voltammetric signals even corresponding to larger than single-monolayer coverage (more than one Ru per terpy-C6-SAc ligand in a densely packed monolayer), Section 3.1.3. Addition of exogenous bipy ligand towards completion of the coordination sphere of terpy-bound Ru(II)/(III), however, led to better defined voltammograms and sub-monolayer but still high (65%) surface coverage. Based on the voltammetric data, the terpy-SAc surface layers with bound Ru(II)/(III) were therefore also addressed by *in situ* STM, with focus on *in situ* scanning tunnelling current/overpotential and bias voltage spectroscopy rather than *in situ* STM imaging.

Fig. 12A shows a representative tunnelling current/overpotential correlation of the Ru-bound terpy-SAc complex at constant bias voltage. No exogenous ligand has been added. The working electrode overpotential scanning showed hysteresis. Potential scanning towards negative potentials displayed a clear maximum around −0.2 V, whereas the reverse scan showed a "dissipative", featureless correlation. This behaviour was reversible in the sense that successive reversible scans showed repetitively the same pattern.

The STS spectra were, however, recorded during rapid potential sweeps. This may account for the slow rise in the

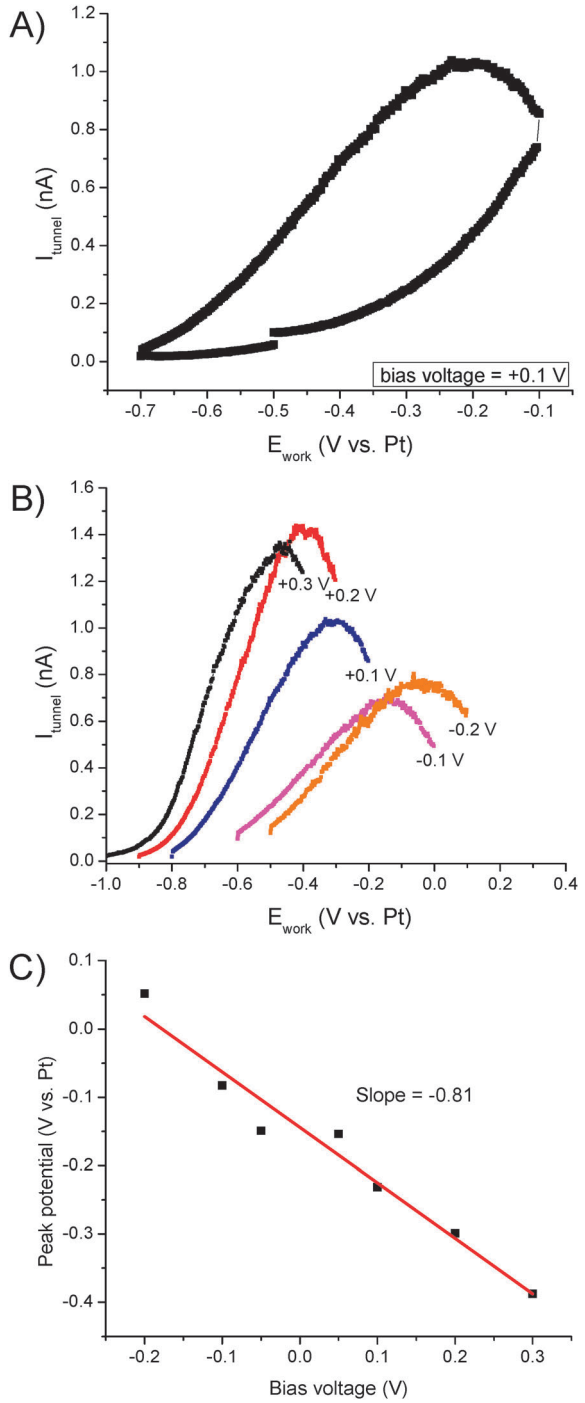

Fig. 12 STS of terpy-C6-SAc on a Au(111) electrode further functionalized by $RuCl_3$ in 0.01 M KH_2PO_4/K_2HPO_4 (pH 7.0). (A) Tunnelling current/overpotential correlation at constant bias voltage of 0.1 V, *i.e.* parallel variation of the working electrode and tip potential relative to the common reference electrode. (B) Tunnelling current/overpotential correlations at different bias voltages, ranging from −0.2 V to 0.3 V. For the negative bias voltages the modulus of the negative current values has been taken to aid presentation of the STS-spectra side-by-side. (C) Plot of the peak potentials in the tunnelling current at different bias voltages. Reference electrode Pt (0.20–0.25 V *vs.* SCE at pH 7.0).

current during the forward sweep which is then followed by a peak in tunnelling current during the reverse (negative-going) scan. Slow charge state switching of the Ru(II)/(III) couple (which must be accompanied by counter-ion charge movement) in the nano-gap between the STM tip and metal substrate could be a rationale for the effect.

The maximum follows expectations from recently developed theoretical approaches to single-molecule *in situ* STM of *redox*, as opposed to non-redox molecules.[19–25] The position of the maximum is ideally expected at the equilibrium redox potential but this can be significantly modified if finite size confinement, ionic strength, detailed tunnelling gap potential distribution and other factors are incorporated. Systematic variation of the peak potential with the bias voltage is, however, generally expected as the molecular redox centre is exposed to part of the bias voltage drop in the tunnelling gap.

Such dependence is displayed in Fig. 12B. The peak potential is systematically displaced towards negative potentials as the bias voltage is increased from −0.1 V to +0.3 V. This observation testifies to the operation of two-step electron transfer between the working electrode and the tip *via* the Ru-based redox centre, with temporary population of the intermediate redox level. We shall address this mechanism further in Section 4.

4. Discussion

We have studied the self-assembly of pure and mixed monolayers of sulfur-linked metal-coordinated terpy on Au(111)-electrode surfaces. The immobilized terpy functional group has shown to be suitable for coordination of the three metals Os, Fe and Ru as disclosed by CV and *in situ* STM. Monolayer voltammetry of transition metal complexes have been reported[38–43] before but with a very few exceptions[10–14] using only polycrystalline electrode surfaces. *Ex situ* STM of transition metal complexes has also been reported,[44–48] but *in situ* STM under full electrochemical potential control to single-molecule resolution are still very few.[10–14] In addition, the approach of *in situ* preparation of the metal-coordinated monolayers has emerged as very efficient.

In situ coordination of the three metals and the emerging CV and *in situ* STM displayed rather different patterns. All the three metals coordinated rapidly as reflected in the rapidly evolved (sub)monolayer voltammograms. This is perhaps unexpected for Os, known to be robust to ligand substitution. The Os-terpy complexes displayed well-behaved voltammograms from which coverages around 15% and fast interfacial electrochemical ET rate constants (3–50 s^{-1}) could be determined. Addition of an exogenous bipy ligand towards completion of the Os-coordination sphere evoked characteristic shoulders suggestive of more than a single surface species but well-behaved voltammograms remained.

Iron appeared also to coordinate to surface-immobilized terpy-C6-SAc and well-defined sub-monolayer voltammograms to emerge. The surface coverage of Fe-coordinated terpy-based complex was, however, much smaller than for Os and Ru. Fe-coordination was therefore not pursued in the present study. Reasons for this were noted above. Ru displayed the most efficient coordination. Initial Ru(III)-binding aroused strong but composite monolayer voltammograms with coverages well in excess of a dense single monolayer. The voltammograms, however, sharpened notably and reduced

to monolayer coverage (65%) on addition of exogenous bipy ligand, indicative of more selective formation of a single monolayer species only.

All the rate constant have values within an order of magnitude or so. With polypyridine ligands none of the three transition metals are expected to be subject to major intramolecular reorganization, although this is less clear for the remaining three, water, chloro- or hydroxo-ligands. Further, the magnitude is in the expected range for example for a total solvent reorganization free energy of about 0.5 eV and weak tunnelling constraints, say a transmission coefficient of 0.01–0.1.[19,49,50] A larger reorganization free energy can be counter-acted by a larger transmission coefficient that can reach the adiabatic limit of unity. These values accord with observed values for other transition metal complexes and redox metalloproteins.

The voltammetric patterns of the *in situ* prepared Os- and Fe-complexes were supported by *in situ* STM under electrochemical potential control. Dense background monolayers, presumably from uncomplexed terpy-C6-SAc were observed in either case. No molecular structures could be observed for the Fe-complex but pits ranging in size from that of a single molecule to several nanometers were observed, indicative of Au-S chemical interaction. The latter was supported by the equilateral triangular shape of the pits following the underlying Au(111)-atomic structure. The Os-complex showed much stronger molecular scale structures evenly distributed over the surface. These were assigned to two-step interfacial ET channels by successive reduction and re-oxidation of the Os-centre such as extensively reported elsewhere, both experimentally[1–4,10–17,19] and supported theoretically.[19,21–25,37] The surface coverage of the strong contrasts accords with the coverage observed from the voltammetric data. The almost complete absence of strong contrasts for the Fe-complex also corresponds to the much lower voltammetric coverage of this complex.

The low coverages of the Fe- and even the Os-complex are not suitable for approaches to (single-molecule) *in situ* tunnelling current/overpotential and bias voltage spectroscopy as widely dispersed single-molecule structures are hard to localize on repeated scanning. The high-coverage Ru-complex was therefore chosen for *in situ* STS (Fig. 12). *In situ* STS displayed systematically the strong maximum in the tunnelling current/overpotential correlation around the voltammetric equilibrium potential and a systematic, approximately linear shift of the peak potential with the bias voltage as expected for a two-step incoherent ET mechanism.[11,12,17,19–25] The slope of the correlation was 0.8 (overpotential/bias voltage). A combination of ionic strength and electrical potential distribution effects in the tunnelling gap is inherent in this quantity[23,24] and will be addressed elsewhere.

The tunnelling peaks were accompanied by hysteresis in reversible scanning. This effect was less apparent in the voltammetric scans. STS involved, however, fast sweeps in a nanogap configuration whereas the CV recording was relatively slow. This difference could therefore be indicative of kinetically controlled ligand substitution features. The maximum in the anodic scan direction remained, however, robust. Prompted by the voltammetric data that pointed strongly towards sharper and better defined voltammograms on exogenous ligand addition, similar completion of the ligand sphere of the Ru-complex in the *in situ* STM tunnelling gap is presently being pursued.

In conclusion, robust voltammetry of the three *in situ* prepared immobilized terpy-based complexes testify to the perspective of this approach. The approach could be improved and extended by addition of exogenous ligands. Further extension can be envisaged by using other metals such as manganese, copper or vanadium. The approach could be taken to the single-molecule level of resolution by *in situ* STM. This offers other perspectives in combination with biological marking where the conductivity of biological molecules can be addressed in this way.

Acknowledgements

Financial support of this work by the Villum Kann Rasmussen Foundation is gratefully acknowledged. We are also grateful to the Otto Mønsted Foundation for a visiting professorship to Professor Richard J. Nichols. Professor Jesper Wengel and PhD.-student Kasper Kannegaard Karlsen, University of Southern Denmark are acknowledged for helpful discussions.

Notes and references

1 W. Haiss, R. J. Nichols, H. van Zalinge, S. J. Higgins, D. Bethell and D. J. Schiffrin, *Phys. Chem. Chem. Phys.*, 2004, **6**, 4330–4337.
2 W. Haiss, T. Albrecht, H. van Zalinge, S. J. Higgins, D. Bethell, H. Hobenreich, D. J. Schiffrin, R. J. Nichols, A. M. Kuznetsov, J. Zhang, Q. Chi and J. Ulstrup, *J. Phys. Chem. B*, 2007, **111**, 6703–6712.
3 R. J. Nichols, W. Haiss, D. G. Fernig, H. van Zalinge, D. J. Schiffrin and J. Ulstrup, in In situ *STM Studies of Immobilized Biomolecules at the Electrode-Electrolyte Interface*, ed. O. Hammerich and J. Ulstrup, *Bioinorganic Electrochemistry*, Springer, Dordrecht, 2008, pp. 207–247.
4 Z. Li, B. Han, G. Meszaros, I. Pobelov, T. Wandlowski, A. Blaszczyk and M. Mayor, *Faraday Discuss.*, 2006, **131**, 121–143.
5 D. M. Kolb, *Angew. Chem., Int. Ed.*, 2001, **40**, 1162–1181.
6 I. Willner and E. Katz, *Angew. Chem., Int. Ed.*, 2000, **39**, 1180–1218.
7 J. He, Q. Fu, S. M. Lindsay, J. W. Ciszek and J. M. Tour, *J. Am. Chem. Soc.*, 2006, **128**, 14828–14835.
8 N. Tao, *Phys. Rev. Lett.*, 1996, **76**, 4066–4069.
9 F. Chen, J. Hihath, Z. Huang, X. Li and N. J. Tao, *Annu. Rev. Phys. Chem.*, 2007, **58**, 535–564.
10 B. Q. Xu, P. M. Zhang, X. L. Li and N. J. Tao, *Nano Lett.*, 2004, **4**, 1105–1108.
11 T. Albrecht, A. Guckian, J. Ulstrup and J. G. Vos, *Trans. IEEE*, 2005, **4**, 430–434.
12 T. Albrecht, A. Guckian, J. Ulstrup and J. G. Vos, *Nano Lett.*, 2005, **5**, 1451–1455.
13 A. M. Ricci, E. J. Calvo, S. Martin and R. J. Nichols, *J. Am. Chem. Soc.*, 2010, **132**, 2494–2495.
14 S. Yoshimoto and K. Itaya, *J. Porphyrins Phthalocyanines*, 2007, **11**, 313–333.
15 Q. Chi, O. Farver and J. Ulstrup, *Proc. Natl. Acad. Sci. U. S. A.*, 2005, **102**, 16203–16208.
16 Q. Chi, J. Zhang, P. S. Jensen, H. E. M. Christensen and J. Ulstrup, *Faraday Discuss.*, 2006, **131**, 181–195. Faraday Discussions, 2006, 131, Molecular Wires and Nanoscale Conductors, Manchester, 2005.
17 E. Della Pia, Q. Chi, D. D. Jones, J. E. MacDonald, J. Ulstrup and M. Elliot, *Nano Lett.*, 2011, **11**, 176–182.
18 A. C. Welinder, J. Zhang, D. B. Stensgaard and J. Ulstrup, *Phys. Chem. Chem. Phys.*, 2010, **12**, 9999–10011.

19 J. Zhang, A. M. Kuznetsov, I. G. Medvedev, Q. Chi, T. Albrecht, P. S. Jensen and J. Ulstrup, *Chem. Rev*., 2008, **108**, 2737–2791.
20 A. M. Kuznetsov and J. Ulstrup, *J. Phys. Chem. A*, 2000, **104**, 11531–11540 *Errata*: J. Phys. Chem. A, 2001, **105**, 7494.
21 J. Zhang, A. M. Kuznetsov and J. Ulstrup, *J. Electroanal. Chem*., 2003, **541**, 133–146.
22 J. Zhang, Q. Chi, A. M. Kuznetsov, A. G. Hansen, H. Wackerbarth, H. E. M. Christensen, J. E. T. Andersen and J. Ulstrup, *J. Phys. Chem. B*, 2002, **106**, 1131–1152.
23 I. G. Medvedev, *J. Electroanal. Chem*., 2007, **600**, 151–170.
24 A. M. Kuznetsov, I. G. Medvedev and J. Ulstrup, *J. Chem. Phys*., 2007, **127**, 104708.
25 T. Albrecht, A. Guckian, A. M. Kuznetsov, J. G. Vos and J. Ulstrup, *J. Am. Chem. Soc*., 2006, **128**, 17132–17138.
26 M. Kalek, A. S. Madsen and J. Wengel, *J. Am. Chem. Soc*., 2007, **129**, 9392–9400.
27 *Charge Transfer in DNA: From Mechanism to Application*, ed. H.-A. Wagenknecht, Wiley-VCH, Weinheim, 2005.
28 E. L. S. Wong and J. J. Gooding, *Langmuir*, 2005, **21**, 6957–6965.
29 J. C. Genereux and J. K. Barton, *Chem. Rev*., 2010, **110**, 1642–1662.
30 J. J. Gooding, *Euroanalysis*, 2002, **14**, 1149–1156.
31 T. Albrecht, K. Moth-Poulsen, J. B. Christensen, A. Guckian, T. Bjørnholm, J. G. Vos and J. Ulstrup, *Faraday Discuss*., 2006, **131**, 265–279. Faraday Discussions **131**: Molecular Wires and Nanoscale Conductors, Manchester, 2005.
32 Q. Chi, J. Zhang, W. P. Friis, J. E. T. Andersen and J. Ulstrup, *Electrochem. Commun*., 1999, **1**, 91–96.
33 J. Zhang, Q. Chi, J. U. Nielsen, E. P. Friis, J. E. T. Andersen and J. Ulstrup, *Langmuir*, 2000, **16**, 7229–7237.
34 H. B. Gray and J. R. Winkler, *Proc. Natl. Acad. Sci. U. S. A*., 2005, **102**, 3534–3539.
35 H. B. Gray and J. R. Winkler, *Q. Rev. Biophys*., 2003, **36**, 341–372.
36 B. K. Ghosh and A. Chakravorty, *Coord. Chem. Rev*., 1989, **95**, 239–294.
37 A. V. B. Cruz, A. K. Mishra and W. Schmickler, *Chem. Phys*., 2010, **371**, 10–15.
38 A. L. Eckermann, D. J. Feld, J. A. Shaw and T. J. Meade, *Coord. Chem. Rev*., 2010, **254**, 1769–1802.
39 T. J. Meyer and M. H. V. Huynh, *Inorg. Chem*., 2003, **42**, 8140–8160.
40 A. Ricci, C. Rolli, S. Rothacher, L. Baraldo, C. Bonazzola, E. J. Calvo, N. Tognalli and A. Fainstein, *J. Solid State Electrochem*., 2007, **11**, 1511–1520.
41 K. Yokoyama, A. Wakabayashi, K. Noguchi, N. Nakamura and H. Ohno, *Inorg. Chim. Acta*, 2006, **359**, 807–814.
42 J. L. Brennan, T. E. Keyes and R. J. Forster, *Langmuir*, 2006, **22**, 10754–10761.
43 Z. Wang, M. J. Cook, A.-M. Nygård and D. A. Russell, *Langmuir*, 2003, **19**, 3779–3784.
44 J. Park, A. N. Pasupathy, J. I. Goldsmith, C. Chang, Y. Yaish, J. R. Petta, M. Rinkoski, J. P. Sethna, H. D. Abruña, P. L. McEuen and D. C. Ralph, *Nature*, 2002, **417**, 722–725.
45 W. Deng and K. W. Hipps, *J. Phys. Chem. B*, 2003, **107**, 10736–10740.
46 D. Natelson, L. H. Yu, J. W. Ciszek, Z. K. Keane and J. M. Tour, *Chem. Phys*., 2006, **324**, 267–275.
47 L. C. Mayor, A. Saywell, G. Magnano, C. J. Satterley, J. Schnadt and J. N. O'Shea, *J. Chem. Phys*., 2009, **130**, 164704.
48 K. Seo, A. V. Konchenko, J. Lee, G. S. Bang and H. Lee, *J. Am. Chem. Soc*., 2008, **130**, 2553–2559.
49 A. M. Kuznetsov and J. Ulstrup, *Electrochim. Acta*, 2000, **45**, 2339–2361.
50 A. M. Kuznetsov and J. Ulsttrup, *Electron Transfer in Chemistry and Biology. An Introduction to the Theory*, Wiley, Chichester, 1999.